Natural Resources Canada
Ressources naturelles Canada

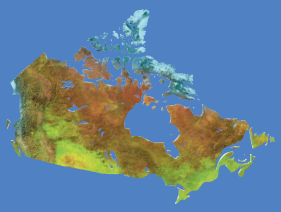

Primary and secondary ore textures in the West Ansil volcanic-hosted massive-sulphide deposit, Noranda mining camp, Rouyn-Noranda, Quebec

S.M. Boucher, M.D. Hannington, and B. Dubé

Geological Survey of Canada

Current Research 2010-10

2010

Canada

Geological Survey of Canada
Current Research 2010-10

Primary and secondary ore textures in the West Ansil volcanic-hosted massive-sulphide deposit, Noranda mining camp, Rouyn-Noranda, Quebec

S.M. Boucher, M.D. Hannington, and B. Dubé

2010

ISSN 1701-4387
Catalogue No. M44-2010/10E-PDF
ISBN 978-1-100-16614-8
DOI 10.4095/286047

A copy of this publication is also available for reference in depository libraries across Canada through access to the Depository Services Program's Web site at http://dsp-psd.pwgsc.gc.ca

A free digital download of this publication is available from GeoPub: http://geopub.nrcan.gc.ca/index_e.php

Toll-free (Canada and U.S.A.): 1-888-252-4301

Recommended citation

Boucher, S.M., Hannington, M.D., and Dubé, B., 2010. Primary and secondary ore textures in the West Ansil volcanic-hosted massive-sulphide deposit, Noranda mining camp, Rouyn-Noranda, Quebec; Geological Survey of Canada, Current Research 2010-10, 16 p.

Critical review
P. Mercier-Langevin

Authors

S.M. Boucher
(sbouc016@uottawa.ca)
M.D. Hannington
(mark.hannington@uottawa.ca)
Ottawa-Carleton Geoscience Centre
University of Ottawa
140 Louis Pasteur
Ottawa, Ontario K1N 6N5

B. Dubé
(Benoit.Dube@RNCan-NRCan.gc.ca)
Geological Survey of Canada
490, rue de la Couronne
Québec, Quebec G1K 9A

Correction date:

Primary and secondary ore textures in the West Ansil volcanic-hosted massive-sulphide deposit, Noranda mining camp, Rouyn-Noranda, Quebec

S.M. Boucher, M.D. Hannington, and B. Dubé

Boucher, S.M., Hannington, M.D., and Dubé, B., 2010. Primary and secondary ore textures in the West Ansil volcanic-hosted massive-sulphide deposit, Noranda mining camp, Rouyn-Noranda, Quebec; Geological Survey of Canada, Current Research 2010-10, 16 p.

Abstract: The West Ansil deposit is the first copper discovery in 25 years in the Noranda central camp. It has a combined indicated and inferred resource of about 1.2 Mt. Grades for the indicated resource are 3.4% Cu, 0.4% Zn, 1.4 g/t Au, and 9.2 g/t Ag. Locally, gold grades are up to 10 ppm within massive chalcopyrite ore, which is significantly higher than other central camp deposits (e.g. Corbet). The bulk of the resource is located in three massive-sulphide lenses (upper, middle, and lower) that are hosted in the Rusty Ridge unit above the Lewis exhalite. The Lewis exhalite is a key marker that is also related to the nearby Ansil mine (1.58 Mt, 8.03% Cu, 0.09% Zn) about 1.8 km northeast of the West Ansil deposit. The overall distribution of massive-sulphide ore and stringer zones at the West Ansil deposit suggests either stacking of separate lenses or dissection of a single deposit by late-stage faulting and dyke formation. The mineralization in all three ore lenses consists of massive pyrrhotite+chalcopyrite±magnetite. Semimassive sphalerite is restricted to the upper and lower parts of the middle lens. Massive magnetite occurs in the upper and middle lenses, where it replaces massive pyrrhotite. A striking feature of the West Ansil deposit is the presence of abundant colloform and nodular pyrite (±marcasite) in the massive-sulphide deposits, especially at the top and bottom of the main massive-sulphide lens. The colloform pyrite is interpreted to be a product of supergene alteration of pyrrhotite. This alteration may be related to shearing at the contacts of the lenses that allowed penetration of groundwater into the massive-sulphide deposits.

Résumé : Le gisement de West Ansil représente la première découverte de cuivre des 25 dernières années dans le camp central de Noranda. Il renferme des ressources indiquées et présumées totalisant environ 1,2 Mt. La teneur des ressources indiquées est de 3,4 % Cu, 0,4 % Zn, 1,4 g/t Au et 9,2 g/t Ag. Par endroits, les teneurs en or atteignent 10 ppm dans du minerai de chalcopyrite massive, une teneur considérablement plus élevée que celle d'autres gisements du camp central (p. ex. Corbet). La majeure partie de la ressource se trouve dans trois lentilles de sulfures massifs (lentilles supérieure, médiane et inférieure) encaissées dans l'unité de Rusty Ridge, sus-jacente à l'exhalite de Lewis. L'exhalite de Lewis est un repère clé qui est également lié à la mine Ansil (1,58 Mt, 8,03 % Cu, 0,09 % Zn) située à proximité, à environ 1,8 km au nord-est du gisement de West Ansil. La répartition générale du minerai et des faisceaux de filonnets de sulfures massifs dans le gisement de West Ansil laisse supposer soit un empilement de lentilles distinctes, soit la dissection d'un seul gisement par la formation de failles et de dykes de phase tardive. Dans les trois lentilles de minerai, la minéralisation se compose principalement de pyrrhotite+chalcopyrite ±magnétite massives. La sphalérite semi-massive se limite aux parties supérieure et inférieure de la lentille médiane. La magnétite massive est présente dans les lentilles supérieure et médiane, où elle remplace la pyrrhotite massive. Une caractéristique marquante du gisement de West Ansil est la présence abondante de pyrite (±marcasite) colloforme et nodulaire dans les sulfures massifs, particulièrement au sommet et à la base de la principale lentille de sulfures massifs. Selon notre interprétation, la pyrite colloforme serait le produit d'une altération supergène de la pyrrhotite. Cette altération pourrait être liée au cisaillement aux contacts des lentilles, qui aurait permis la pénétration des eaux souterraines dans les sulfures massifs.

INTRODUCTION

The West Ansil deposit is hosted by volcanic rocks of the Blake River Group, one of several Archean volcanic complexes that form the Abitibi greenstone belt of the southern Superior Province (Baragar, 1968; Dimroth et al., 1982; Gélinas et al., 1984). The deposit lies conformably in volcanic stratigraphy in the central part of the central camp, 6 km north of Rouyn-Noranda (Fig. 1). The orebody was discovered in 2005 by Xstrata Copper Canada Ltd. and is the first significant new base-metal discovery in the central camp in 25 years. The deposit occurs at the basalt-andesite contact within the Rusty Ridge unit in the Noranda camp and is the only known massive sulphide at this stratigraphic level (Fig. 2). The original drill targets were characterized by the presence of a significant alteration zone near the intersection of two recognized synvolcanic faults within the Rusty Ridge formation. Historical drillholes that intersected the alteration did not reach the Lewis contact, the deep horizon at which the nearby Ansil deposit was found, or the stratigraphic position of the Corbet deposit next to the Flavrian intrusion (Xstrata Copper Canada Ltd., 2005); however, several off-hole geophysical anomalies (borehole electromagnetic) were found stratigraphically above the interpreted position of the Lewis contact. These were subsequently targeted for drilling in 2005, and significant Cu-rich stringer mineralization and massive-sulphide deposits were intersected in three separate zones. The combined upper, middle, and lower lenses of the West Ansil deposit have indicated and inferred resources of about 1.2 Mt with grades for the indicated resource of 3.4% Cu, 0.4% Zn, 1.4 g/t Au, and 9.2 g/t Ag (Xstrata Copper Canada Ltd., 2005).

Like the Ansil deposit, the West Ansil deposit differs from the other massive-sulphide deposits of the central camp (e.g. Riverin and Hodgson, 1980; Riverin et al., 1990; Cattalani et al., 1993) in the following ways: 1) the bulk of the orebody is Cu-rich and Zn-poor and dominated by chalcopyrite and pyrrhotite; 2) massive magnetite forms a significant portion of the deposit; 3) there is a lack of conspicuous alteration around the middle lens; and 4) abundant late-stage colloform pyrite±marcasite overprints the massive pyrrhotite. This paper documents the main ore types of the West Ansil deposit, as well as metal zonation and the overall paragenesis, and discusses possible explanations for the high Cu/Cu+Zn ratios, the abundant magnetite, and the unusual late-stage pyrite and marcasite.

GEOLOGICAL SETTING OF THE WEST ANSIL DEPOSIT

Regional geology

The Blake River Group in the Noranda area is 12–15 km thick and composed of bimodal mafic and felsic volcanic rocks with rapid facies changes and a marked variation in the thicknesses of individual units (de Rosen-Spence, 1976; Gibson and Watkinson, 1990; Riverin et al., 1990). The Noranda volcanic complex is approximately 2.7 Ga and measures 35 km in diameter and 7.5–9 km in thickness. It is dominated by the Noranda cauldron and shield volcano (Gibson and Watkinson, 1990), which consists of rhyolitic, andesitic, and basaltic flows and minor pyroclastic rocks (Mortensen, 1987; Gibson and Watkinson, 1990). The volcanic rocks have been metamorphosed to the greenschist facies, although some areas include higher or lower grade rocks. The volcanic rocks of the Noranda volcanic complex have been divided into five cycles, each consisting of an andesitic to basaltic basal unit and mixed rhyolite and andesite upper unit (Gibson and Watkinson, 1990). Cycle 3, also referred to as the mine sequence, is host to most of the massive-sulphide deposits of the Noranda central camp and consists of a bimodal succession of tholeiitic basalt to rhyolite, interpreted to have erupted during periods of cauldron subsidence within the upper central part of the Noranda shield volcano (Gibson and Watkinson, 1990). The overall stratigraphic setting of the Blake River Group has recently been revised by Goutier et al. (2009) based on detailed U-Pb geochronology (e.g. McNicoll et al., (2009). The mine sequence is now considered to be part of the ca. 2702–2696.7 Ma Noranda rocks (*see* Goutier et al., 2009; McNicoll et al., 2009). The Corbet, Ansil, and West Ansil deposits are the lowest in the mine sequence stratigraphy (Barrett et al., 1991, 1993; Galley, 1994) (Fig. 2). Average grades indicate a generally higher Cu/Cu+Zn ratio (>0.5) for Corbet, Ansil, and West Ansil than for deposits located higher in the stratigraphy (Barrett et al., 1991, 1993)

Local geology

The West Ansil deposit is located within the Rusty Ridge formation, at an andesite-basalt contact, stratigraphically above the Ansil deposit (Fig. 2). The long axis of the deposit trends north and has a strike length of 200 m, with a thickness of approximately 50 m (Fig. 3). The stratigraphy in the immediate vicinity of the deposit includes the Northwest rhyolite, the Rusty Ridge andesite, the Amulet dacite, and the Amulet rhyolite (Fig. 4). These units generally dip toward the east-northeast at approximately 30° to 45°. All of the volcanic units have a dominantly tholeiitic affinity (Barrett et al., 1991). The top of the Northwest rhyolite corresponds to the position of the Lewis exhalite, but this horizon has not been observed at West Ansil. The Rusty Ridge formation, which comprises andesite overlain by basalt, is intruded by the Amulet dacite and rhyolite. The extrusive sequence is underlain by the Flavrian pluton, a composite body of mainly trondhjemitic composition (Goldie, 1978; Gibson and Galley, 2007).

The Rusty Ridge andesite is a dark green, massive, pillowed unit, with chloritized and brecciated flow margins. The pillows are metre-sized and locally contain centimetre-scale quartz- and chlorite-filled amygdales, fracture-filling

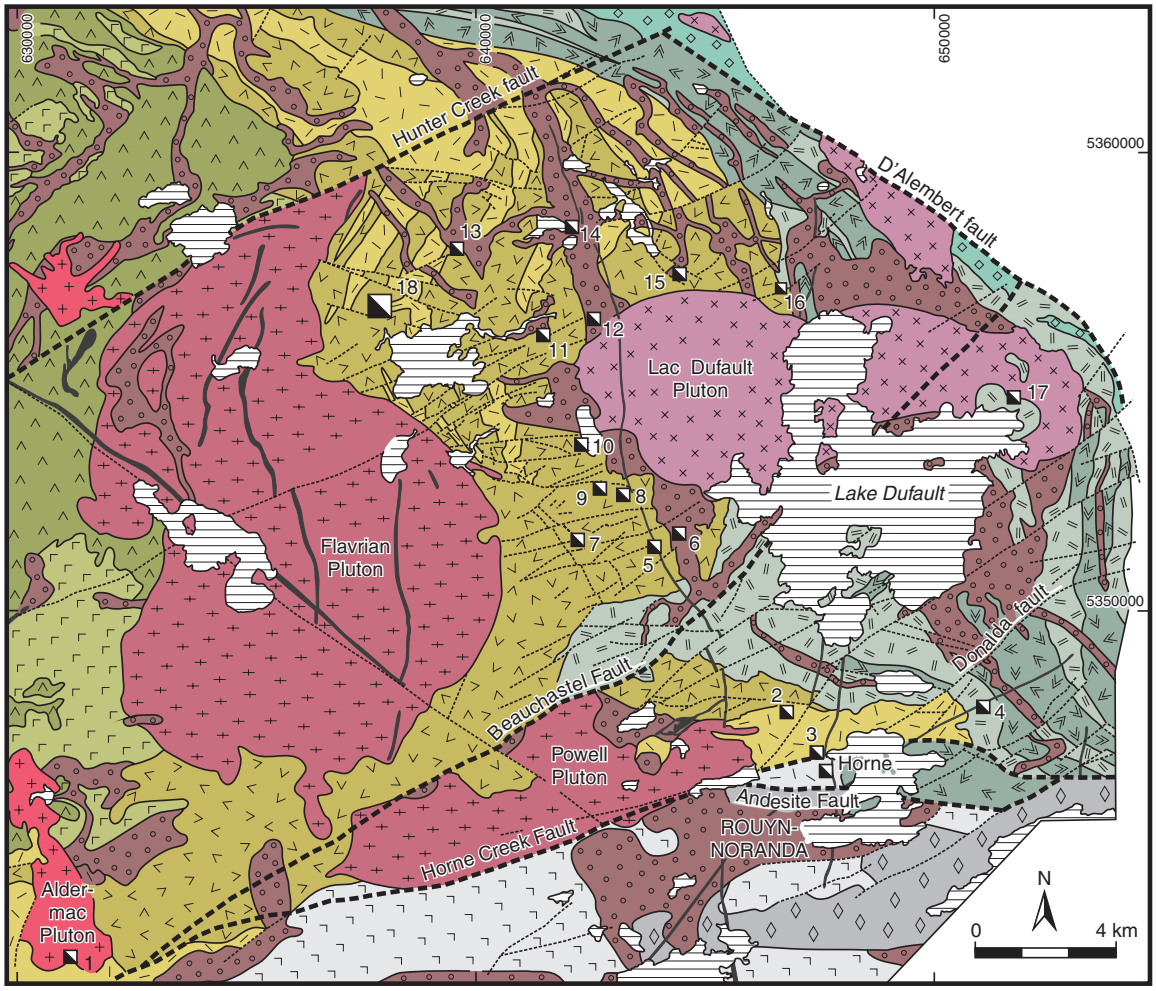

Deposits: 1 = Aldermac, 2 = Joliet, 3 = Quemont, 4 = Delbridge, 5 = D68, 6 = Millenbach, 7 = Corbet, 8 = Amulet A, 9 = Amulet C, 10 = Amulet F, 11 = Old Waite, 12 = East Waite, 13 = Ansil, 14 = Vauze, 15 = Norbec, 16 = Newbec, 17 = Gallen, and 18 = West Ansil

ARCHEAN EXTRUSIVE ROCKS

Undifferentiated
- Rhyolite
- Basalt and/or andesite

Cycle 1+2
- Rhyolite
- Basalt and/or andesite

Cycle 3
- Rhyolite
- Basalt and/or andesite

Cycle 4
- Rhyolite
- Basalt and/or andesite

Cycle 5
- Basalt and/or andesite

ARCHEAN INTRUSIVE ROCKS
- Syenite
- Granodiorite
- Trondhjemite, tonalite
- Gabbro, quartz diorite

PROTEROZOIC INTRUSIVE ROCKS
- Diabase

- Major fault
- Minor fault
- Deposit

Figure 1. Generalized geological map of the Noranda camp, showing the regional geology, major structural elements, as well as the distribution of extrusive and intrusive rocks. West Ansil and other volcanic-hosted massive-sulphide deposits of the mine sequence are also shown (*after* Monecke et al., 2008).

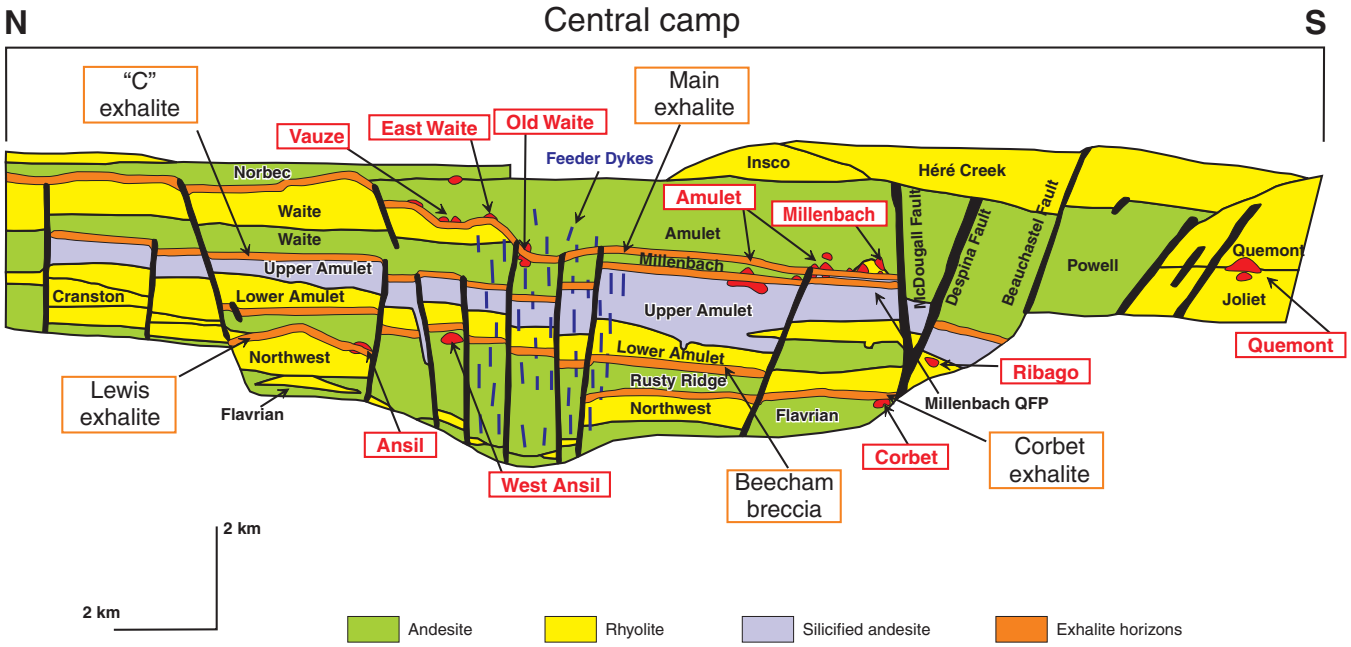

Figure 2. Stratigraphic position of the West Ansil deposit within the reconstructed Noranda cauldron showing the main exhalite horizons, synvolcanic structures, and the significant volcanic-hosted massive-sulphide deposits of the mine sequence (*after* Gibson and Galley, 2007).

chlorite, and disseminated pyrite and chalcopyrite. The flow-breccia units have a distinctly chloritized matrix. The Rusty Ridge basalt is also dark green, with massive to brecciated portions; its upper and lower parts can only be distinguished on the basis of lithogeochemistry (Xstrata Copper Canada Ltd., 2005). The brecciated portion is generally located at the top of the unit. The fragments range from 0.2 cm to 2 cm, with 2–5 volume per cent chlorite-filled amygdales, and the matrix is chloritized and silicified. The massive portion is generally fine grained, and contains 1–2 volume per cent chlorite-filled amygdales ranging from 1–2 mm. The Amulet dacite is pale to medium grey and is characterized by a massive aphanitic texture with rare quartz-filled amygdales and local disseminated pyrrhotite, pyrite, and chalcopyrite. It intrudes the Rusty Ridge formation and generally has brecciated contacts. At West Ansil, the lower contact of the dacite with the Rusty Ridge basalt is discordant, confirming its intrusive nature. Above the Rusty Ridge basalt, the lower Amulet rhyolite is present where the contact is not cut by the dacite. It is aphyric to granular, pale to medium grey, generally massive, with flow breccia, and contains 2–10 volume per cent quartz- and chlorite-filled amygdales. The brecciated facies is composed of clasts from 0.5 cm to 3 cm in a chlorite matrix.

The upper lens and stockwork zone of the West Ansil deposit are located within the upper Rusty Ridge basalt near the contact with the Amulet dacite. The middle lens occurs between the lower Rusty Ridge basalt and andesite. The lower lens and stockwork zone are located at the contact between the lower Rusty Ridge basalt and andesite (Fig. 4). A large, 60 m thick diorite sill separates the middle lens from the lower lens at the approximate location of the basalt-andesite contact. Other smaller diorite sills cut through the West Ansil deposit as well as most of the stratigraphy. A second set of subvertical feldspar porphyritic diorite dykes cut the middle lens and the Rusty Ridge andesite and basalt. They are associated with local recrystallization of sulphide minerals and quartz-carbonate veining (*see* 'West Ansil orebody' section, below).

WEST ANSIL OREBODY

The upper lens of the West Ansil deposit is an ovoid body located at a vertical depth of approximately 160 m with a dip extent of roughly 60 m, a maximum thickness of 30 m, and a width of 25 m (Fig. 3, 4). The dominant sulphide mineral is massive pyrrhotite with minor disseminated chalcopyrite and local chalcopyrite veins. Discontinuous lenses of massive magnetite are present throughout the upper lens, but are more abundant at the top where the thickest intersection of magnetite occurs (Fig. 5). Bands of colloform pyrite and marcasite, up to 30 cm thick, occur along the upper and lower contacts of the lens. A narrow stringer zone extending below the upper lens has a dip extent of about 80 m, a width of 5–10 m, and a length of 25 m. The stringer mineralization consists of chalcopyrite veins and veinlets with minor magnetite in a strongly chloritized black basalt-andesite breccia.

The middle lens represents the bulk of the West Ansil orebody and is located at a vertical depth of 285 m with a dip extent of 160 m, a width of about 50 m, and a thickness of 45 m at its centre and 5–8 m at its outer edge (Fig. 4). The lens consists mainly of massive pyrrhotite with minor disseminated chalcopyrite that surrounds a chalcopyrite-rich

core. Semimassive sphalerite also occurs within massive pyrrhotite in the upper western part of the lens. Minor massive magnetite is restricted to the lower part. A conspicuous feature of the massive-sulphide mineralization of the middle lens is the presence of abundant, partially replaced siliceous and chloritic wall-rock fragments (pseudobreccia). These are interpreted to represent relict clasts of basalt or andesite, possibly along flow contacts, that were infiltrated by the massive sulphide (*see* 'Principal ore types' section). Late-stage, colloform pyrite-marcasite nodules and bands up to 30 cm thick are present along the upper and lower contacts of the lens. Minor stringer-like mineralization occurs along the lower contact of the massive-sulphide minerals, but any obvious pipe-like stockwork zone appears to have been cut out by the diorite sill or it was never developed (Fig. 5). The middle lens also lacks conspicuous footwall or hanging-wall alteration along most of its lower and upper contacts. A reactivated synvolcanic fault parallel to the lower contact and diorite sill may have removed any footwall alteration from below the main massive-sulphide lens. This fault also appears to offset the lower lens from the middle lens.

Two small satellite bodies occur directly below the main diorite sill above the lower lens. These bodies are subhorizontal and relatively small, with a combined thickness of only 10 m and a width of approximately 25 m. The larger lower lens is about 20 m thick and 25 m wide and is located at a vertical depth of 485 m. It is relatively flat with a shallow plunge toward the west (Fig. 4). Massive chalcopyrite mineralization is dominant toward the bottom of this lens and grades into more pyrrhotite-rich massive sulphide with disseminated chalcopyrite at the top. Minor colloform pyrite-marcasite nodules and bands occur along the upper and lower contacts, as in the other lenses.

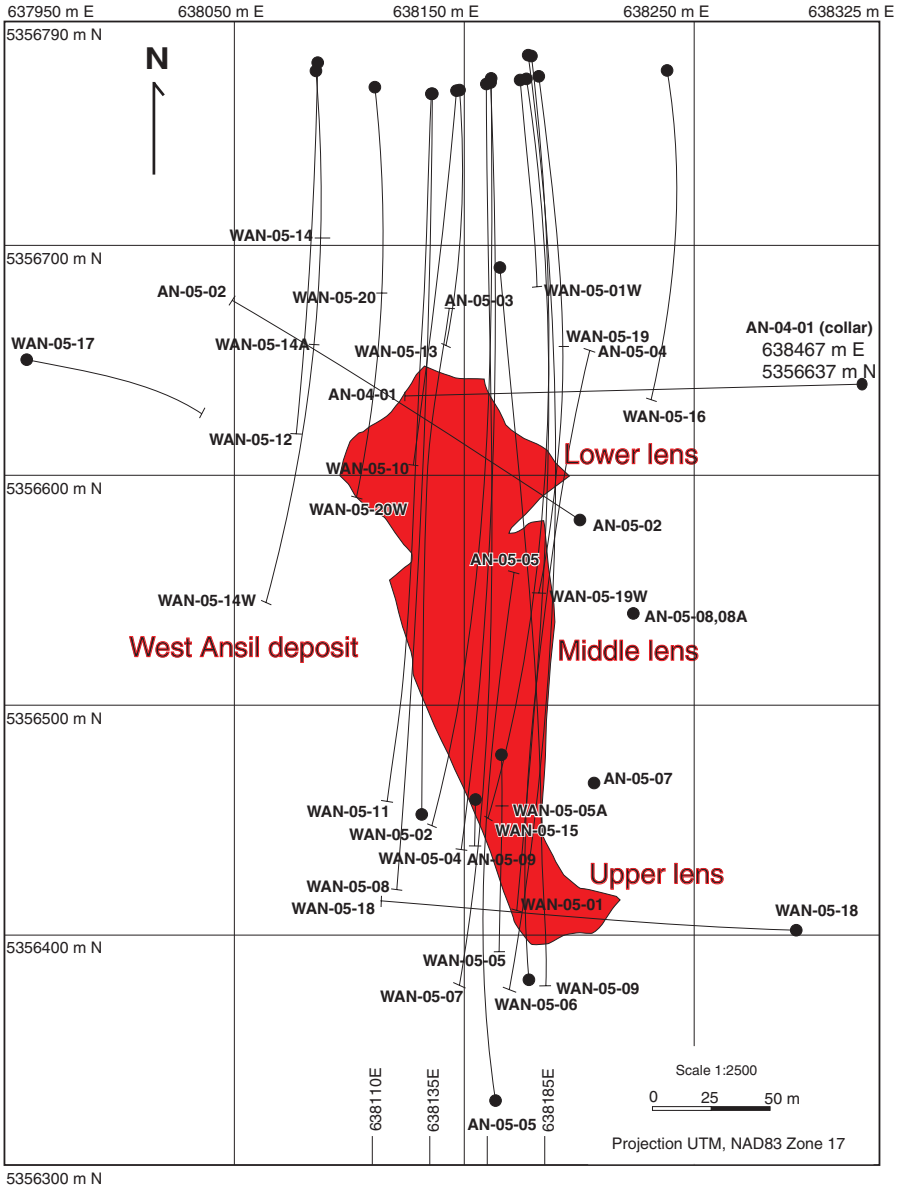

Figure 3. Surface orebody projection of the West Ansil deposit showing the location of drillholes as well as the position of north-south cross-sections in Figure 3b (*modified from* Xstrata Copper Canada Ltd., 2005).

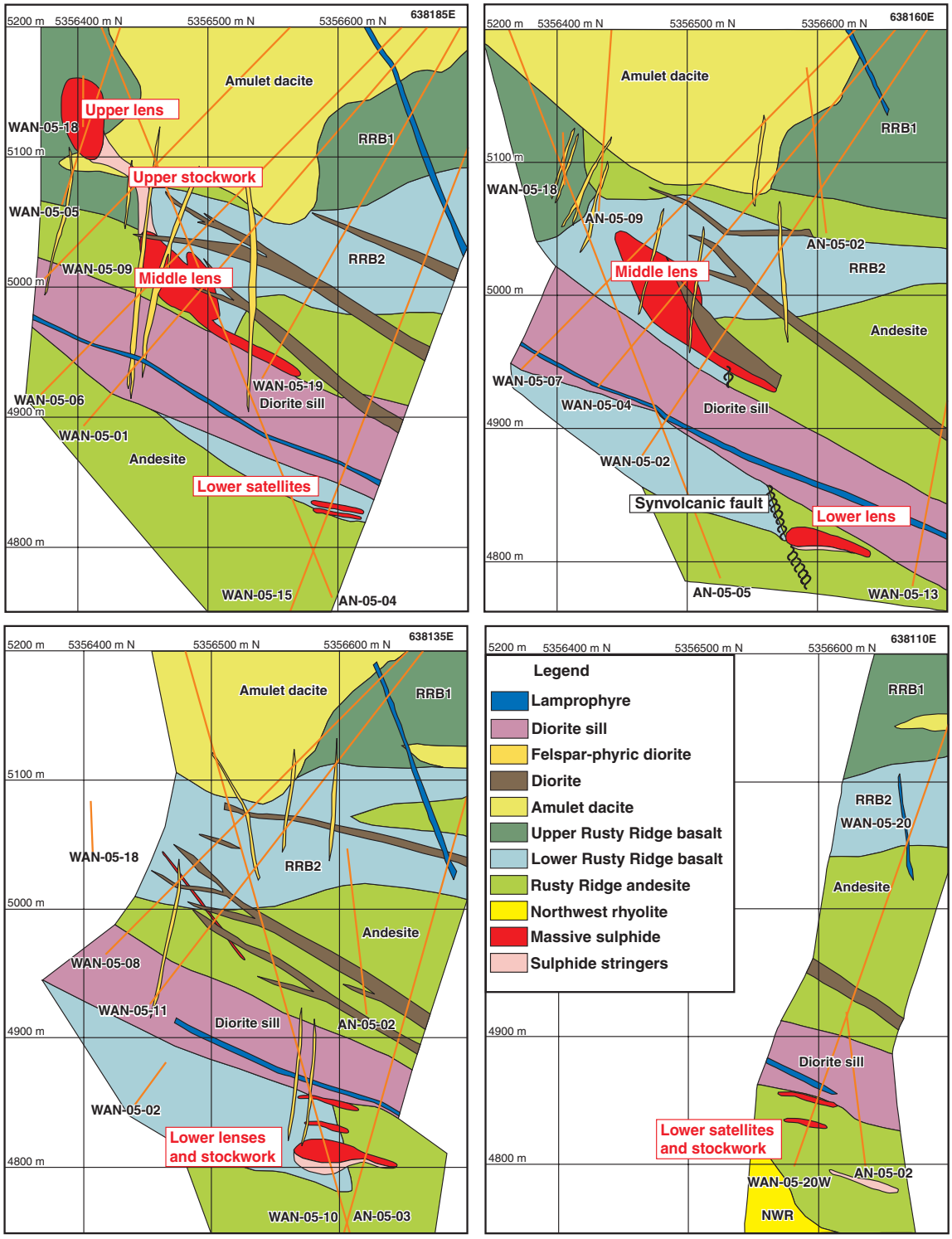

Figure 4. North-south cross-sections (facing west) through the West Ansil deposit showing the position of the upper, middle, and lower lenses. Local stratigraphic units including the Rusty Ridge basalt and andesite, Amulet dacite, as well as diorite sills and subvertical dykes are shown. Logged and sampled drillholes are indicated (*modified from* Xstrata Copper Canada Ltd., 2005).

The lower stockwork zone is located directly below the lower massive-sulphide lens and has an approximate thickness of 20 m and a width of 25 m. The stockwork consists of massive centimetre-scale chalcopyrite veins as well as network-like veinlets within strongly chloritized and silicified fragmental rocks, including hyaloclastite (Fig. 5). Sphalerite stringers occur toward the top of the stockwork zone and are overprinted by chalcopyrite veins and veinlets.

Principal ore types

Representative photographs and illustrations of the different ore types are shown in Figure 6 and Figure 7.

Massive pyrrhotite-chalcopyrite ore

Massive pyrrhotite-chalcopyrite ore is the most common ore type in all three sulphide lenses. The massive ore contains up to 90 olume per cent fine-grained pyrrhotite with 1–5 volume per cent fine-grained disseminated chalcopyrite (Fig. 6a, b). Chalcopyrite also occurs as wispy, planar to contorted discontinuous bands up to several centimetres wide (Fig. 7a). Contacts between alternating bands of chalcopyrite and pyrrhotite are sharp and smooth to serrate. Rounded millimetre-scale siliceous grains are abundant within the chalcopyrite-rich bands and wisps. Pseudobreccia zones are present throughout the massive-sulphide lenses and along footwall and hanging-wall contacts. They consist of angular fragments or clasts of chloritic or siliceous material (partially replaced wall rock) in a matrix of pyrrhotite and chalcopyrite (Fig. 6c 7b, c). The less well defined siliceous clasts, with intense pyrrhotite replacement, locally grade into more angular centimetre-scale chloritized fragments within a more or less continuous fine-grained chalcopyrite±sulphide matrix (Fig. 7b, c). These fragments commonly have alteration rims with projections of pyrrhotite or chalcopyrite into the fragments. Massive chalcopyrite is also locally concentrated at the upper and lower contacts of the massive-sulphide lenses separating the massive pyrrhotite from the strongly

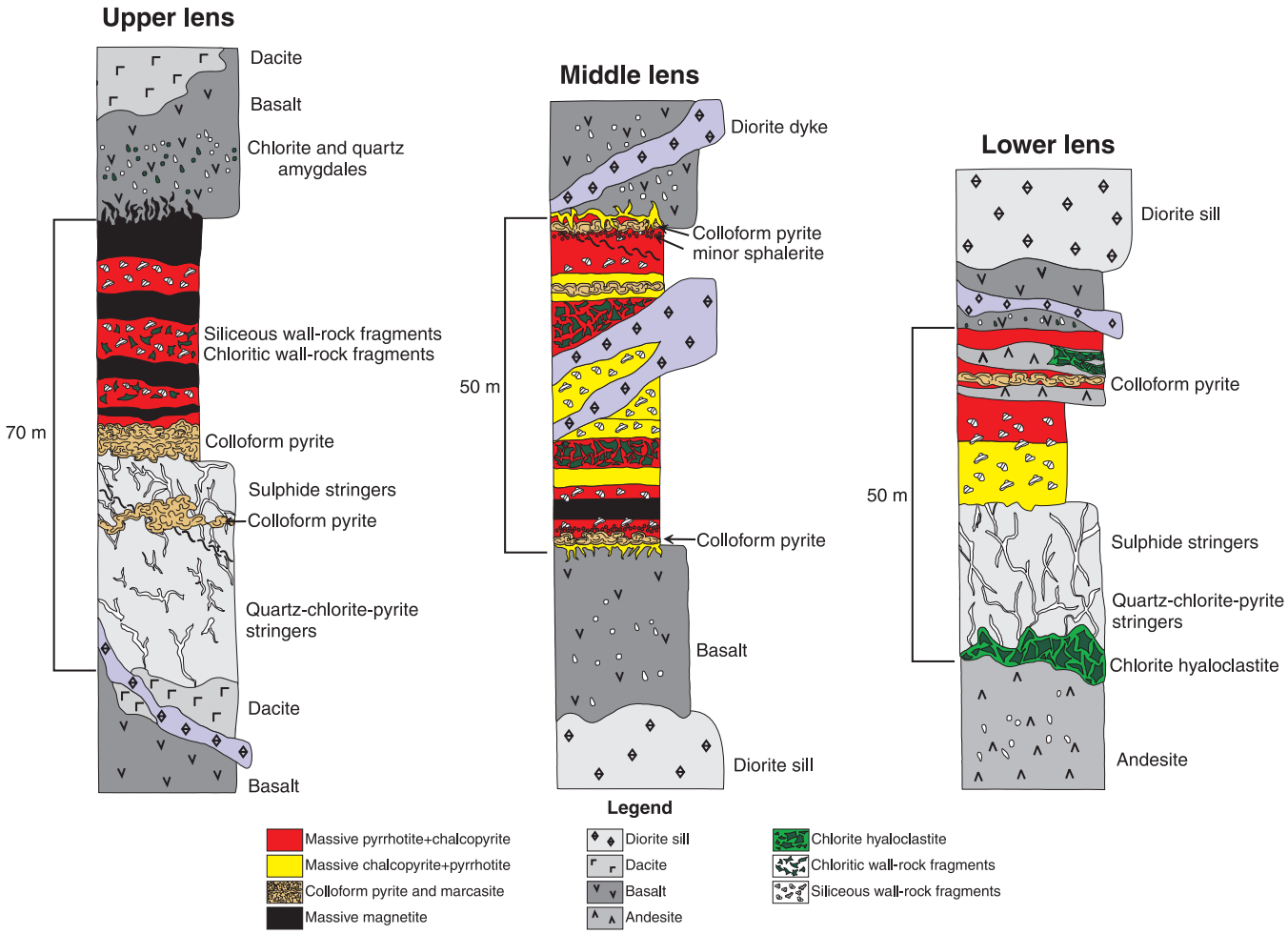

Figure 5. Composite graphic logs of the upper, middle, and lower lenses of the West Ansil deposit showing the dominant massive-sulphide ores and stockwork zones, contact relationships, the main mafic volcanic units, and major mafic dykes intruding the lenses. Note that the scale is intended to show the thickness of each lens, but not of the units in the lenses.

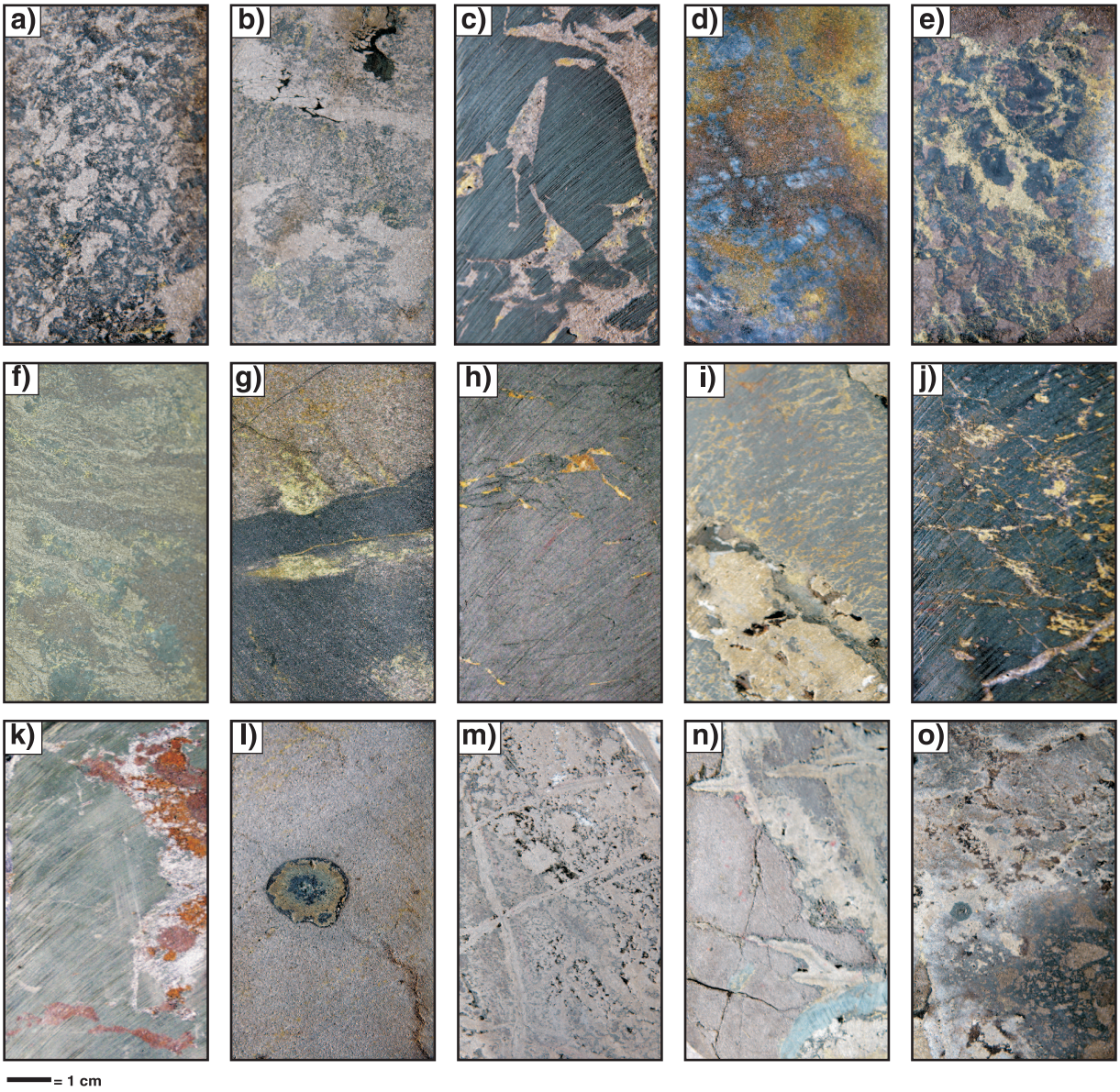

Figure 6. Representative photographs of drill-core samples showing sulphide ore textures in the West Ansil lenses. **a)** Partially pyrrhotite-replaced silicified and chloritized basalt pseudobreccia from the upper lens. 2010-190. **b)** Silicified-chloritized basalt pseudobreccia, almost completely replaced by massive pyrrhotite±chalcopyrite from the lower lens. 2010-189. **c)** Strongly chloritized basalt breccia in a pyrrhotite-rich matrix from the middle lens. 2010-193. **d)** Massive chalcopyrite±pyrrhotite ore with partially replaced siliceous fragments from the lower lens. 2010-186. **e)** Partially replaced siliceous fragments in a chalcopyrite±pyrrhotite matrix from the middle lens. 2010-192. **f)** Massive pyrrhotite±sphalerite with chalcopyrite in the middle lens showing millimetre- to centimetre-scale semicontinuous sphalerite-rich bands. Rounded microcrystalline quartz fragments are also present and appear to be the product of strong silicification. 2010-194. **g)** Magnetite bands in massive pyrrhotite±chalcopyrite from the upper lens. 2010-187. **h)** Massive magnetite with remobilized chalcopyrite veinlets from the upper lens. 2010-191. **i)** Massive magnetite in pyrrhotite±chalcopyrite with colloform pyrite-marcasite replacing pyrrhotite adjacent to the magnetite. Chalcopyrite has been remobilized into late fractures developed in the brittle magnetite. 2010-200. **j)** Chalcopyrite stringer in silicified-chloritized basalt from the lower stockwork zone. 2010-188. **k)** Sphalerite-pyrrhotite stringer in chloritized basalt from the bottom of the middle lens. 2010-196. **l)** Isolated secondary pyrite-marcasite nodule in massive pyrrhotite from the upper lens. 2010-199. **m)** Porous massive colloform pyrite-marcasite from the middle lens. 2010-198. **n)** Fracture-controlled recrystallized pyrite in colloform pyrite replacing massive pyrrhotite from the middle lens. 2010-195. **o)** Colloform pyrite-marcasite replacing the pyrrhotite-rich matrix of silicified basalt pseudobreccia from the middle lens. 2010-197. All photographs by S. Boucher.

chloritized basalt and andesite. Centimetre-scale colloform pyrite-marcasite nodules selectively replace the pyrrhotite where late fractures penetrate the massive-sulphide lenses (Fig. 7d, e, f).

Massive chalcopyrite-pyrrhotite ore

Massive chalcopyrite-rich ore occurs in the central part of the middle lens and dominates the lower lens. The massive ore contains up to 70 volume per cent fine-grained anhedral chalcopyrite with 20 volume per cent disseminated pyrrhotite (Fig. 6d). Chalcopyrite is present as large centimetre-scale continuous to discontinuous bands alternating with millimetre-scale bands of pyrrhotite (Fig. 7g). Locally, chalcopyrite, pyrrhotite, and sphalerite are intergrown, with about 50 volume per cent chalcopyrite, 30 volume per cent pyrrhotite, and 20 volume per cent sphalerite in some parts of the middle lens; however, pyrrhotite inclusions in chalcopyrite-rich bands suggest that the chalcopyrite may have replaced earlier massive pyrrhotite. As in the pyrrhotite-rich ore, the chalcopyrite appears to have replaced brecciated basalt, with unreplaced silicified and chloritized remnants of basalt locally preserved in the massive chalcopyrite and pyrrhotite (Fig. 6e).

Massive pyrrhotite-sphalerite ore

Sphalerite-rich ores are most common in the upper western part of the middle lens in association with massive pyrrhotite. The sphalerite occurs as millimetre- to centimetre-scale discontinuous to contorted bands in the massive pyrrhotite. Minor chalcopyrite is also present within the sphalerite bands, replacing both pyrrhotite and sphalerite (Fig. 6f). Contacts between sphalerite and pyrrhotite bands appear gradational, whereas contacts between chalcopyrite and pyrrhotite are sharp (Fig. 7h). Sphalerite is also present with pyrrhotite in the matrix of pseudobreccia zones, cementing partially replaced siliceous and chloritic wall-rock fragments. Minor remobilized chalcopyrite locally replaces the pyrrhotite-sphalerite-rich matrix along the contacts with the siliceous fragments.

Massive magnetite

Massive magnetite occurs at the top of the upper lens and as a 5 m thick pod near the bottom of the middle lens. At the top of the upper lens the massive magnetite is characterized by re-entrant cusps and centimetre-scale projections of magnetite into the strongly chloritized hanging-wall basalt progressing into disseminated magnetite that extends 15 cm into the basalt above the massive magnetite contact (Fig. 7i). Quartz-carbonate-chlorite veins and veinlets also extend into the hanging wall, which appear to be co-precipitating with magnetite (Fig. 5, 7i). In the main sulphide bodies the massive magnetite is fine grained and occurs in centimetre- to metre-scale bands of 60–90 volume per cent magnetite alternating with pyrrhotite (Fig. 6g). Quartz, chlorite, and actinolite are the dominant gangue minerals associated with the massive magnetite zones. Locally, siliceous and chloritic fragments occur as fine breccia in a matrix of magnetite (Fig. 6h, 7j). Inclusions of pyrrhotite are common in the magnetite and suggest that the magnetite replaced the pre-existing pyrrhotite (Fig. 7k). Chalcopyrite is abundant as disseminated grains in massive magnetite and especially as millimetre-scale veinlets; the latter appears to have been structurally remobilized into brittle fractures in the massive magnetite and along magnetite-pyrrhotite contacts (Fig. 6i, 7l). Colloform pyrite and marcasite are also commonly present replacing pyrrhotite along the contacts of the massive magnetite (Fig. 7m).

Chalcopyrite stringer mineralization

The chalcopyrite stringer mineralization below the upper and lower lenses occurs in two distinct styles: network-like stringers and massive chalcopyrite±pyrrhotite veins within strongly chloritized hyaloclastite and basalt-andesite breccia. The fine, network-like stringers occupy an extensive zone of microfractures within the chloritic basalt-andesite beneath each of the sulphide lenses, as well as beneath the massive chalcopyrite-pyrrhotite vein stockwork zones and extends a few metres above the middle and lower sulphide lenses (Fig. 5, 6j). Larger chalcopyrite±pyrrhotite veins predominate in the centre of the upper and lower stockwork zones, where individual veins can be up to 20 cm wide, often with cores or rims of pyrrhotite (Fig. 7n). The more pyrrhotite-rich stringers typically occur in the upper stockwork zone (below the upper lens). Both fine network-like stringers and larger veins contain chlorite and quartz which increase in abundance laterally and horizontally away from the core of the main chalcopyrite stockwork zones (Fig. 7o). Minor chalcopyrite stringers are also present directly below the middle sulphide lens, but a stockwork zone appears to be missing at this location (Fig. 5).

Sphalerite stringer mineralization

A network of millimetre- to centimetre-scale sphalerite stringers occurs mostly in the lower stockwork zone (below the lower lens) and locally in the immediate footwall of the middle lens where it is not cut by diorite. Individual veins of sphalerite are up to several centimetres wide within strongly chloritized hyaloclastite and basalt or andesite breccia. Minor pyrrhotite is also present in the sphalerite stringers and appears to have replaced sphalerite (Fig. 7p). Some sphalerite stringers contain euhedral millimetre-sized pyrite grains. In the lower stockwork zone, sphalerite stringers occur outside the chalcopyrite-rich core of the stockwork mineralization, but are cut by chalcopyrite-pyrrhotite veinlets (Fig. 6k).

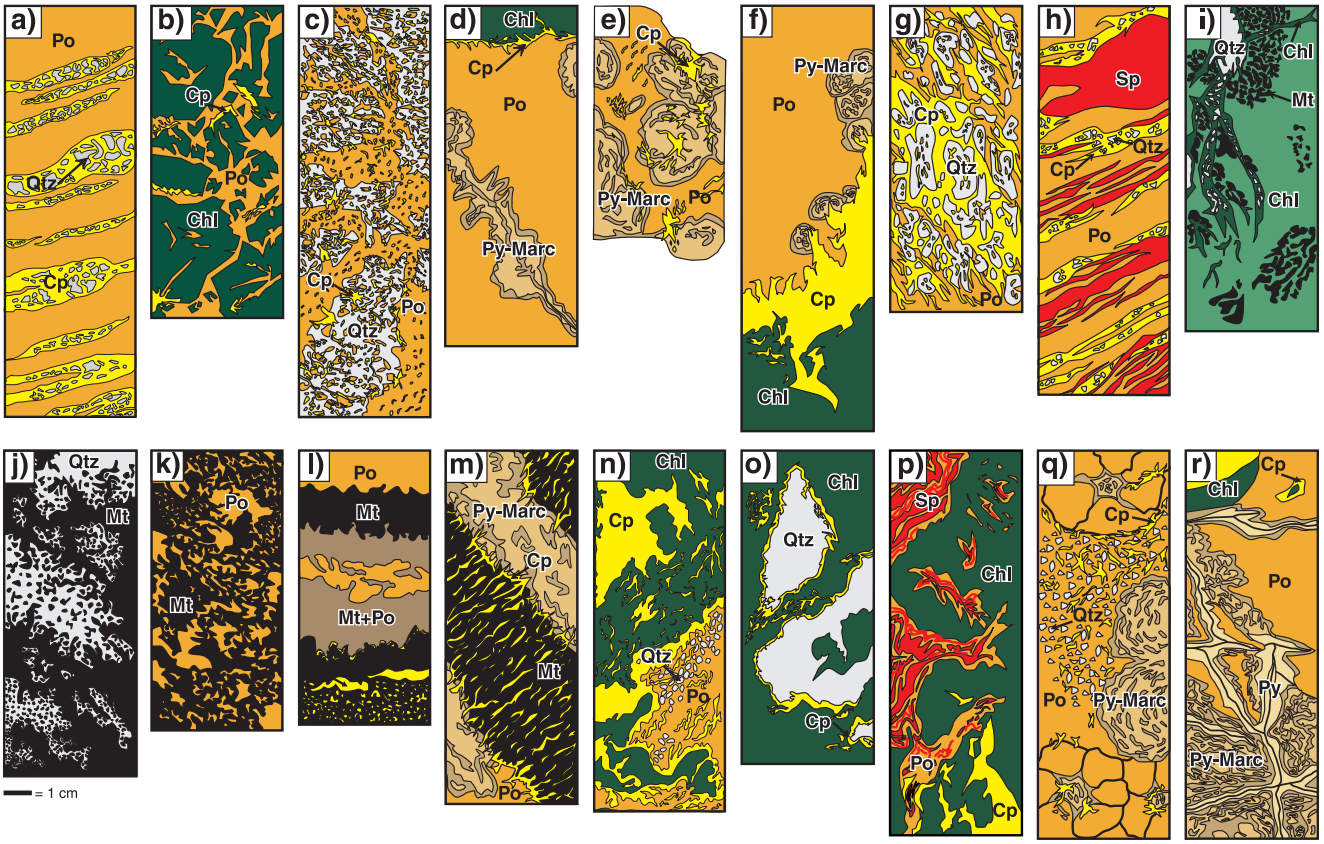

Colloform pyrite-marcasite

Bands or lenses of nodular and colloform pyrite and marcasite occur mostly at the top and bottom of all three sulphide lenses. The bands consist of fine-grained pyrite-marcasite intergrowths that form centimetre-sized spheroidal bodies (Fig. 6l) or clots and locally coalesce to form 5–40 cm thick porous layers that replace massive pyrrhotite (Fig. 6m, 7q). The initial stages of replacement appear to be characterized by clover-leaf shapes formed by the coalescence of small neighbouring clots of pyrite and marcasite; these acted as nuclei for larger nodular growths (Fig. 7q). Typically, the pyrite-marcasite growths are centred on fractures in the pyrrhotite, and colloform bands or layers develop parallel to the fractures (Fig. 6n, 7r). Contacts between the pyrite-marcasite and massive pyrrhotite are characterized by the presence of 'skrinkage cracks' indicating volume loss, where dark brown siliceous material separates both sulphide minerals. The dark brown material is interpreted to be hisingerite, which is an amorphous iron-silicate mineral commonly formed as a secondary product of weathering of pyrrhotite-rich ore (Murowchick, 1992; *see* 'Evolution of the massive sulphide lenses' section). It occurs locally as centimetre-scale bands around the pyrite-marcasite nodules and also contains desiccation cracks. Recrystallized pyrite is present within late fractures in some colloform bands, possibly indicating late-stage fluid circulation. Locally, the pyrite and marcasite nodules are surrounded by a carbonate- and quartz-rich matrix (Fig. 6o). At the top of the middle lens, remobilized sphalerite and galena fill late open spaces within and between the nodular pyrite-marcasite crusts. Minor remobilized chalcopyrite also occurs between nodules or colloform bands and along pyrite-marcasite and pyrrhotite contacts (Fig. 7q, r).

Metal zonation

Ore assays from 1 m long core splits were used to construct metal zonation profiles of the upper, middle, and lower lenses. The Cu, Zn, Au, Ag, and Pb concentrations in 16 drillholes from all three lenses were plotted on composite sections in Figure 8. Metal contents in the West Ansil deposit do not show a consistent stratigraphic zonation of a Cu-rich base to a Zn-rich top, except in the upper part of the middle lens. The upper lens has an ambiguous zonation apparently caused by the late-stage emplacement of massive magnetite.

The upper lens has a Cu-rich core (3–6 weight per cent Cu), with up to 8 weight per cent Cu in the stockwork zone. High Au (up to 8 ppm) and Ag (up to 15 ppm) also occur in the Cu-rich core, consistent with a strong positive correlation between Cu, Au, and Ag throughout the deposit. Higher concentrations of Ag (up to 20 ppm) were also found in the Cu-rich stockwork zone. The Zn (<0.2 weight per cent) and Pb (<0.01 weight per cent) grades are very low throughout the upper lens; however, Zn values up to 1 weight per cent are present in the stockwork zone. Neither Au nor Ag shows any correlation with Zn. The massive magnetite zone is barren (Fig. 8a).

Figure 7. Schematic illustrations of ore textures in the West Ansil deposit. **a)** Banded pyrrhotite-chalcopyrite (Po-Cp) ore showing discontinuous centimetre-scale chalcopyrite-rich bands containing rounded, partly replaced siliceous wall-rock fragments (Qtz = quartz). Contacts between pyrrhotite and chalcopyrite are sharp and smooth to serrate. The pyrrhotite also contains fine-grained disseminated chalcopyrite and sphalerite. **b)** Chlorite-rich (Chl) basalt breccia from the middle lens with abundant pyrrhotite (Po) in the matrix between angular and partially replaced fragments of black chloritized basalt. The pyrrhotite matrix also contains minor disseminated chalcopyrite (Cp) and remobilized chalcopyrite along the boundaries of chlorite fragments. **c)** Intensely silicified basalt and andesite pseudobreccia from the middle lens with abundant pyrrhotite (Po) and lesser chalcopyrite (Cp) in the matrix between large centimetre-scale angular and almost completely replaced siliceous clasts (Qtz). The quartz-rich fragments appear to be the product of very strong silicification of basalt. Both pyrrhotite and chalcopyrite invade the fragments; however, late chalcopyrite also replaces pyrrhotite. **d)** Massive sulphide at the top of the middle lens with remobilized chalcopyrite (Cp) separating the chloritized (Chl) hanging-wall basalt from the massive pyrrhotite (Po). Remobilized chalcopyrite-rich stringers extend into both the pyrrhotite and the wall rock. The massive pyrrhotite is also partly replaced by centimetre-scale colloform pyrite-marcasite (Py-Marc) nodules and veins centred on late fractures. **e)** Colloform pyrite-marcasite (Py-Marc) in massive pyrrhotite from the middle lens. The large centimetre-scale pyrite-marcarite nodules contain unreplaced pyrrhotite (Po) and late-stage remobilized chalcopyrite (Cp) in shrinkage cracks. **f)** Massive sulphide at the bottom of the middle lens with remobilized chalcopyrite (Cp) separating the chloritized (Chl) footwall basalt from the massive pyrrhotite (Po). Remobilized chalcopyrite-rich stringers extend into both the pyrrhotite and wall rock. Colloform centimetre-scale pyrite-marcasite (Py-Marc) nodules selectively replace the fine-grained pyrrhotite at the lower sulphide contact. **g)** Discontinuous chalcopyrite-rich (Cp) bands from the lower lens alternating with bands of pyrrhotite (Po). Partly replaced siliceous (Qtz) material is present within the bands and is interpreted to represent unreplaced fragments of silicified wall rock. Pyrrhotite inclusions within the chalcopyrite bands suggest that the pyrrhotite was replaced by chalcopyrite, although the present banding is likely tectonic. **h)** Banded pyrrhotite-chalcopyrite±sphalerite (Po-Cp±Sp) ore showing discontinuous millimetre- to centimetre-scale chalcopyrite- and sphalerite-rich bands. Rounded siliceous (Qtz) fragments are present only in the chalcopyrite bands. Contacts between pyrrhotite and chalcopyrite are sharp, whereas contacts between pyrrhotite and sphalerite are more gradational. The pyrrhotite also contains fine-grained disseminated chalcopyrite and sphalerite. **i)** Disseminated magnetite±actinolite grains and clusters within strongly chloritized (Chl) basalt at the top of the upper lens, 10 cm from the massive magnetite (Mt) contact. A quartz-calcite-chlorite (Qtz = quartz) vein appears to cuts the disseminated magnetite and is therefore late. **j)** Massive magnetite (Mt) from the upper lens replacing strongly silicified (Qtz) basalt fragments and forming a continuous matrix in the pseudobreccia. Minor chlorite and actinolite are also overprinted by magnetite. **k)** Massive magnetite (Mt) replacing pyrrhotite (Po) from the upper lens. The massive magnetite contains abundant pyrrhotite inclusions that suggest later introduction of magnetite. **l)** Massive magnetite (Mt) and pyrrhotite (Po) from the upper lens. Massive magnetite generally forms re-entrant cusps into the pyrrhotite. Alternating centimetre-scale bands of pyrrhotite show evidence of extensive remobilization. The magnetite also contains an abundance of disseminated and veinlet chalcopyrite introduced during late remobilization of sulphide minerals into fractures developed in the more brittle magnetite. A chalcopyrite-rich rim occurs at the contact between magnetite and pyrrhotite. **m)** Massive magnetite (Mt) band from the middle lens. The magnetite band appears to crosscut the more massive pyrrhotite. Remobilized chalcopyrite (Cp) veinlets are present throughout the magnetite in late brittle fractures and along the contact with pyrrhotite. Colloform pyrite-marcasite (Py-Marc) along the pyrrhotite-magnetite contact locally replaces pyrrhotite, but not magnetite. **n)** Chalcopyrite-pyrrhotite (Cp-Po) stringer mineralization from the upper stockwork zone. Large centimetre-scale chalcopyrite network-like veins occur within a strongly chloritized (Chl) basalt and appear to have replaced pyrrhotite. Smaller millimetre-scale chalcopyrite veinlets have been locally remobilized into late fractures. Qtz = quartz. **o)** Chlorite (Chl) and minor chalcopyrite (Cp) stringer mineralization in the upper stockwork zone. Centimetre-scale chlorite-actinolite network-like veins occur within a strongly silicified (Qtz) and chloritized basalt breccia. Chalcopyrite rims the siliceous fragments and occurs as microveinlets in the more massive chlorite-actinolite. **p)** Sphalerite (Sp) and pyrrhotite (Po) stringers at the base of the middle lens. The stringers have a rim of pyrrhotite, that may reflect the replacement of early sphalerite stringers by later pyrrhotite. Chl = chlorite, Cp = chalcopyrite. **q)** Colloform pyrite-marcasite (Py-Marc) replacing massive pyrrhotite (Po) in the middle lens. Fracture-controlled centimetre-scale pyrite-marcasite nodules and spheroids are centred on late fractures and invade the massive pyrrhotite. Remobilized chalcopyrite (Cp) also occurs in the late fractures. The radial pattern of some fractures reflects volume loss during replacement of pyrrhotite by pyrite and marcasite. **r)** Colloform pyrite-marcasite (Py-Marc) in massive pyrrhotite (Po) in the middle lens. Replacement of pyrrhotite by centimetre-scale spheroidal bodies of pyrite-marcasite occurs along and between late fractures. Recrystallized pyrite is present within the fractures and remobilized sphalerite fills. Chl = chlorite, Cp = chalcopyrite.

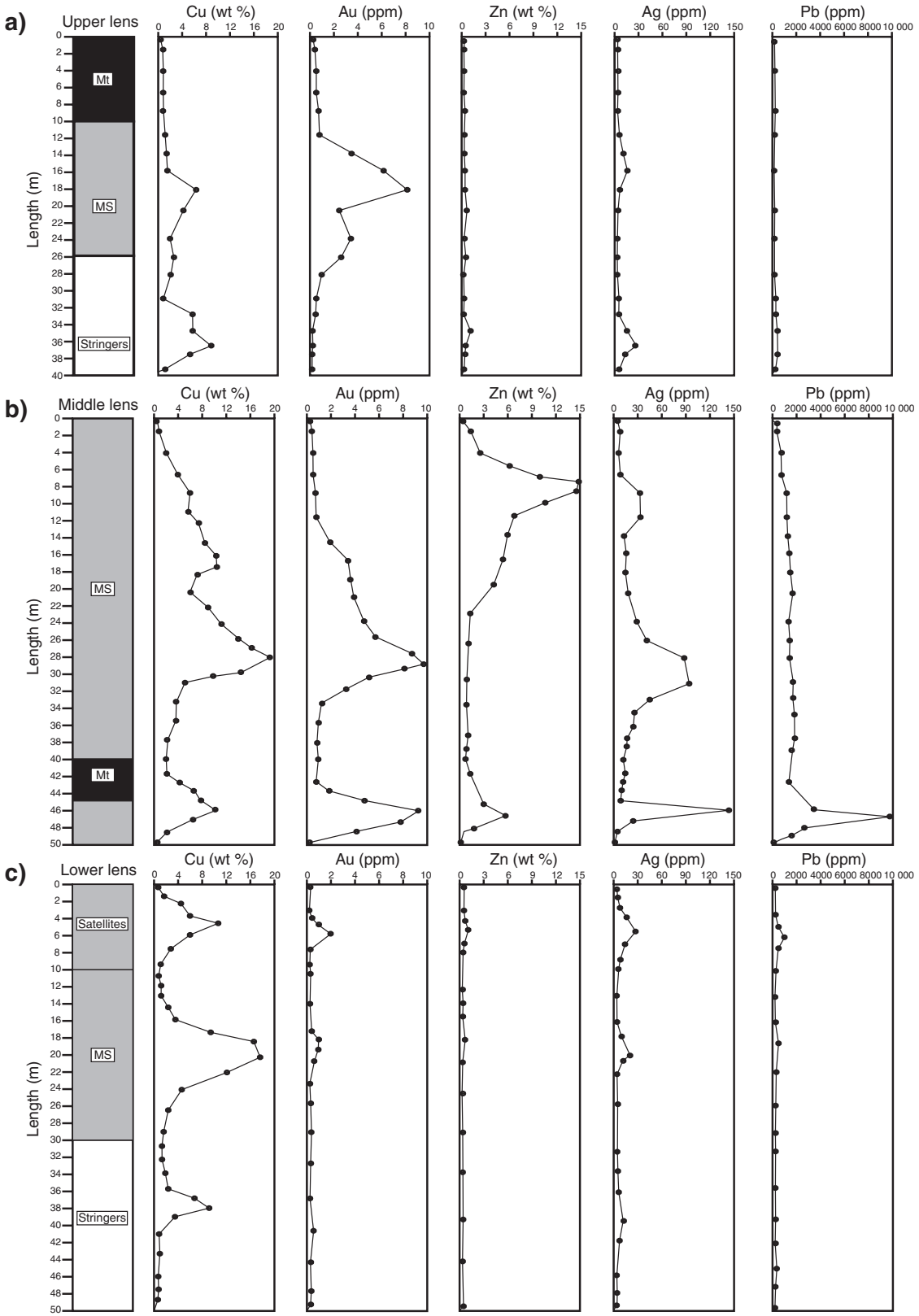
a)
Upper lens
Cu (wt %)
Au (ppm)
Zn (wt %)
Ag (ppm)
Pb (ppm)
Length (m)
Mt
MS
Stringers
b)
Middle lens
Cu (wt %)
Au (ppm)
Zn (wt %)
Ag (ppm)
Pb (ppm)
Length (m)
MS
Mt
c)
Lower lens
Cu (wt %)
Au (ppm)
Zn (wt %)
Ag (ppm)
Pb (ppm)
Length (m)
Satellites
MS
Stringers

The middle lens has a distinctive Zn-rich top (up to 15 weight per cent Zn), Cu-rich core (12–20 weight per cent Cu), and a moderately Cu-rich base and stockwork zone (8–12 weight per cent Cu). Minor Zn (3–6 weight per cent Zn) is also present in the network-like veins at the base of the lens; however, the bulk of the lens contains less than 2 weight per cent Zn. High Au (up to 10 ppm) and Ag (60–150 ppm) are also found in the Cu-rich core and base of the middle lens, supporting the overall Cu-Au-Ag correlation of the deposit. High Pb (~1 weight per cent) occurs at the bottom of the lens and can be explained by remobilized quartz-carbonate-sphalerite-galena veins; however, most of the lens contains less than 0.2 weight per cent Pb. The Au, Ag, and Pb are poorly correlated with Zn, as in the upper lens, and the massive magnetite in the middle lens is barren (Fig. 8b).

The lower lens and stockwork zone are notably Cu-rich, with up to 12 weight per cent Cu in the satellite bodies, 20 weight per cent Cu in the core, and 12 weight per cent Cu in the stringer zone. Gold (2–4 ppm) and silver (15–50 ppm) correlate with the high concentrations of copper. Zinc grades (<1 weight per cent) are very low throughout the lower lens, which could suggest that this was the high-temperature feeder zone of the hydrothermal system. Minor Au, Ag, Pb, and Cu in the satellite bodies can be explained by locally remobilized precious-metal-bearing galena and chalcopyrite (Fig. 8c).

Although the overall gold content of the West Ansil deposit is 1.4g/t, significantly higher grades are found in some parts of the middle lens. The association with high Cu grades is similar to that observed in other deposits of the Central camp such as Ansil and Corbet (Barrett et al., 1991, 1993).

EVOLUTION OF THE MASSIVE-SULPHIDE LENSES

The overall distribution of massive-sulphide ore and stringer zones at the West Ansil deposit suggests either stacking of separate lenses or dissection of a single deposit by late-stage faulting and dyke formation. The presence of a subvertical synvolcanic fault controlling high-temperature stockwork mineralization is suggested by displacement in the volcanic stratigraphy near the lower lens (Fig. 4); however, a stockwork zone beneath the larger middle lens appears to be missing and likely was removed by the massive diorite. The coherent Cu-to-Zn metal zonation in the middle lens suggests that it is intact except for the absence of the stockwork zone. The unusual metal zonation and lack of Zn or Pb enrichment in the upper lens suggests that it might also be out of place (e.g. a faulted portion of the main lens, rather than a stacked lens); however, the presence of the Amulet unit immediately beneath the upper lens is consistent with stacking of lenses. In some sections, there are no obvious subvertical feeders immediately below massive-sulphide parts of the lenses, but semiconformable zones of disseminated sulphide minerals and magnetite are present with semimassive sulphide infilling chlorite-altered hyaloclastite. This suggests that mineralizing fluids may have moved in part laterally through the Rusty Ridge unit, probably through zones of high porosity such as breccia and hyaloclastite (Barrett et al., 1991).

Two stages of mineralization are recognized at the West Ansil deposit: 1) an early stage of sphalerite-pyrrhotite±pyrite mineralization with associated chlorite-quartz alteration, and 2) a later stage of pyrrhotite-chalcopyrite mineralization with magnetite±actinolite replacement. The ore was later subjected to secondary processes that were responsible for colloform pyrite-marcasite replacing pyrrhotite (Fig. 9).

Remnants of the early-stage mineralization (massivebanded sphalerite-pyrrhotite and sphalerite-pyrrhotite-cemented pseudobreccia) occur at the western top of the middle lens. Remnants of sphalerite-pyrrrhotite-rich stringer mineralization within strongly chloritized and silicified andesite also occur locally below the middle lens and at the margins of the lower stockwork zone. Massive sphalerite only occurs at the top of the middle lens, where brecciated basalt is infilled and partly replaced by pyrrhotite and sphalerite. At the nearby Ansil deposit, Galley et al. (1995) interpreted this texture to represent basaltic flows on-lapping the andesite during early-stage hydrothermal activity.

Figure 8. a) Composite metal zonation of the upper lens based on assay data from WAN-05-05, WAN-05-09, and WAN-05-18. The Cu, Au, and Ag show a positive correlation in the centre of the lens and the stockwork zone. The Zn and Pb concentrations are uniformly low. **b)** Composite metal zonation profiles of the middle lens based on assay data from AN-05-04, WAN-05-01, WAN-05-02, WAN-05-04, WAN-05-06, WAN-05-07, and WAN-05-19W. The middle lens has a Zn-rich top and a Cu-rich core and stringer zone. Again, a positive correlation between Cu, Au, and Ag is apparent in the central part of the lens and stringer zone. The high Pb, Zn, Ag, and Au values at the bottom of the lens are due to remobilized galena veins at the basal contact. **c)** Composite metal zonation of the lower lens and stockwork zone based on assay data from AN-05-02, AN-05-03, WAN-05-10, WAN-05-12, WAN-05-15, and WAN-05-20W, including a satellite zone. The Zn and Pb values are low, and Cu, Au, and Ag are positively correlated. MS = massive sulphide, MT = magnetite.

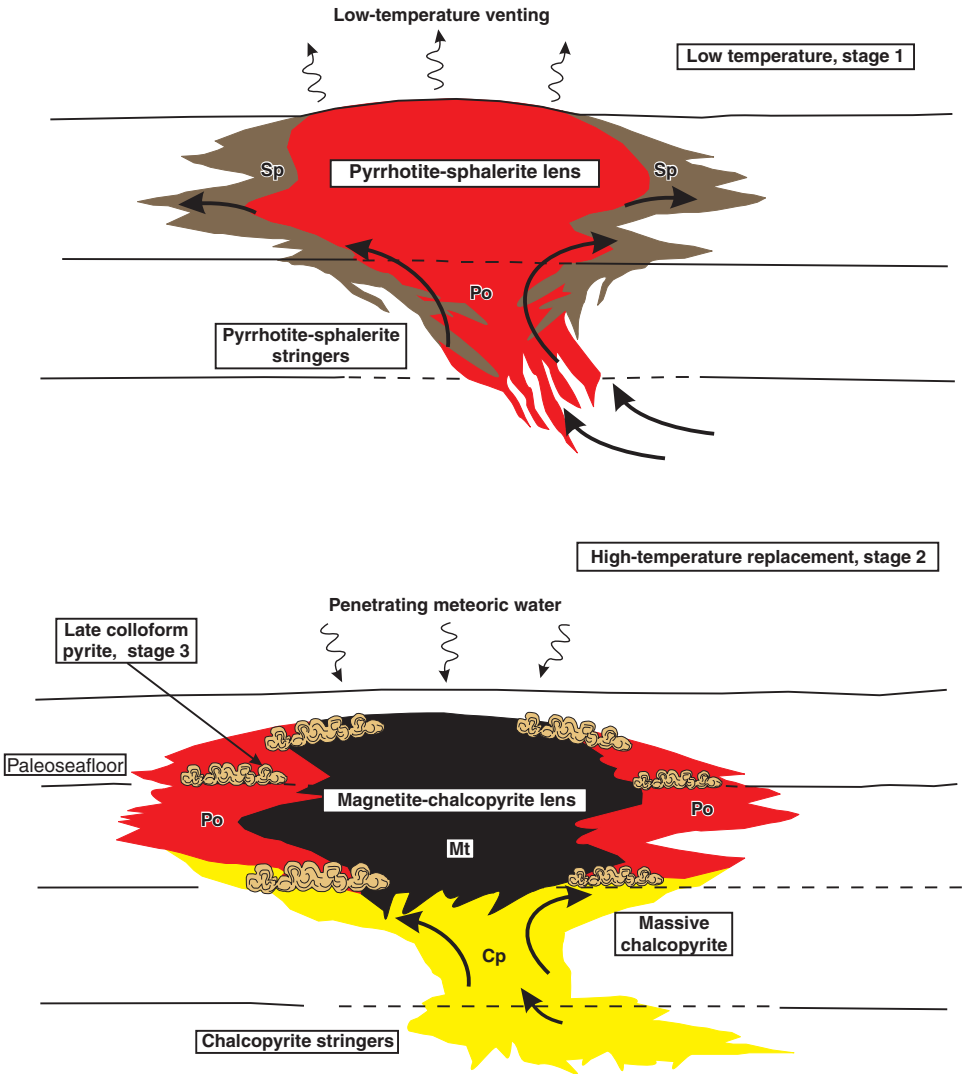

Figure 9. Schematic representation of the development of the West Ansil hydrothermal system. The main stages of mineralization include 1) contruction of a low-temperature sphalerite-pyrrhotite (Sp-Po) vent complex, above a sphalerite-pyrrhotite stockwork; 2) development of late chalcopyrite stringer networks; 3) emplacement of massive chalcopyrite (Cp) and magnetite along a higher temperature replacement front at the base of the sphalerite-pyrite-pyrrhotite lens; and 4) alteration of pyrrhotite along sheared contacts and late fractures and formation of colloform pyrite and marcasite.

The second stage of mineralization involved the development of a pyrrhotite-chalcopyrite vein system below the upper and lower lenses, where the most intense chloritization of the basalt and andesite occurs. The Cu-rich stockworks grade upward into pyrrhotite-chalcopyrite-rich massive sulphide. The middle lens lacks this conspicuous transition, which was most likely removed by the diorite sill that separates the middle lens from the lower lens. The middle and lower lenses both contain a chalcopyrite-rich core which likely formed at peak temperatures in the hydrothermal system (e.g. Barrett et al., 1991). Massive magnetite found in the upper and middle lenses appears to have formed as a replacement of pyrrhotite- and chalcopyrite-rich ore. Magnetite generally forms re-entrant cusps into the massive pyrrhotite and appears to have advanced into or replaced the massive-sulphide minerals, as observed at the Ansil deposit (Riverin et al., 1990; Westendorp et al., 1991; Westendorp, 1992); however, magnetite feeders have not been observed directly below the massive magnetite. Because of its brittle nature, the massive magnetite is commonly veined by remobilized chalcopyrite. At the Ansil deposit, Westendorp (Westendorp et al., 1991; Westendorp, 1992) and Galley et al. (1995, 2000) interpreted the magnetite replacement to have formed when rising hot (350°C) fluids were able to mix with cooler, less acidic, and more oxidized seawater along the footwall and hanging-wall contacts of the massive-sulphide lenses.

Late-stage replacement of massive pyrrhotite by colloform pyrite and marcasite, mostly along the upper and lower contacts of the lenses, appears to be a secondary feature caused by alteration of pyrrhotite along fractures in the ore. The observed nodular and spheroidal pyrite and marcasite closely resemble supergene alteration of massive pyrrhotite in pyrrhotite-rich NiS deposits in other Archean greenstone belts (e.g. Butt and Nickel, 1981). The replacement of massive pyrrhotite by pyrite and marcasite leads to a significant volume reduction, which likely accounts for conspicuous 'shrinkage cracks' associated with the replacement (Fleet, 1978). The amorphous iron oxide, hisingerite, present in these cracks is also a product of sulphide weathering (Murowchick, 1992). This feature is rare in other deposits of the Noranda central camp, but has been described at the New Insco deposit north of Noranda (Larson, 1983). Shearing

and faulting at the contacts of the massive-sulphide lenses at West Ansil may have allowed meteoric water to penetrate into the ore zone to cause pyrrhotite replacement.

Figure 9 illustrates the inferred stages of development of the West Ansil hydrothermal system: 1) construction of a 'low-temperature' sphalerite-pyrrhotite vent complex above a sphalerite-pyrrhotite stockwork, 2) development of higher temperature chalcopyrite stringer networks, 3) emplacement of massive chalcopyrite and magnetite along a replacement front at the base of the sphalerite-pyrrhotite, and 4) alteration of massive pyrrhotite by penetration of groundwater along sheared contacts and late fractures.

The origins of the unusual magnetite-rich zones and the late-stage colloform pyrite and marcasite are being investigated further with detailed chemistry and stable isotopes.

ACKNOWLEDGMENTS

The author would like to thank the personnel at Xstrata Copper Canada Ltd. and Alexis Minerals for providing the geological information such as drill core and Cu-Zn-Ag-Au geochemical data presented in this paper. The author is also grateful to the TGI3-Targeted Geoscience Initiative –3 Abitibi project of the Geological Survey of Canada for their financial support and knowledgeable geological information. Many thanks to M.D. Hannington and T. Monecke for leading the author in the right direction with their assistance in the field, as well as for their academic support.

REFERENCES

Baragar, W.R.A., 1968. Major-element geochemistry of the Noranda volcanic belt, Quebec-Ontario; Canadian Journal of Earth Sciences, v. 5, p. 773–790.

Barrett, T.J., MacLean, W.H., Cattalani, S., Hoy, L., and Riverin, G., 1991. Massive sulfide deposits of the Noranda area, Quebec. III. The Ansil mine; Canadian Journal of Earth Sciences, v. 28, p. 1699–1730.

Barrett, T.J., MacLean, W.H., Cattalani, S., and Hoy, L., 1993. Massive sulfide deposits of the Noranda area, Quebec. V. The Corbet mine; Canadian Journal of Earth Sciences, v. 30, p. 1934–1954.

Butt, C.R.M. and Nickel, E.H., 1981. Mineralogy and geochemistry of the weathering of the disseminated nickel sulfide deposit at Mt. Keith, Western Australia; Economic Geology and the Bulletin of the Society of Economic Geologists, v. 76, p. 1736–1751. doi:10.2113/gsecongeo.76.6.1736

Cattalani, S., Barrett, T.J., MacLean, W.H., Hoy, L., Hubert, C., and Fox, J.S., 1993. Métallogénèse des gisements Hornes et Quemont (region de Rouyn-Noranda); Ministère de l'Énergie et des Ressources du Québec, Rapport ET 90-07, 121 p

de Rosen-Spence, A.F., 1976. Stratigraphy, development and petrogenesis of the Central Noranda volcanic pile, Noranda, Quebec; Ph.D. thesis, University of Toronto, Toronto, Ontario, Canada, 166 p.

Dimroth, E., Imreh, L., Rocheleau, M., and Goulet, N., 1982. Evolution of the south-central part of the Archean Abitibi Belt, Quebec. Part I: stratigraphy and paleogeographic model; Canadian Journal of Earth Sciences, v. 19, p. 1729–1758.

Fleet, M.E., 1978. The pyrrhotite-marcasite transformation; Canadian Mineralogist, v. 16, p. 31–35.

Galley, A.G., 1994. The geology of the Ansil Cu-Zn massive sulphide deposit, Rouyn-Noranda, Quebec; Ph.D. thesis, Carleton University, Ottawa, Ontario, 377 p.

Galley, A.G., Watkinson, D.H., Jonasson, I.R., and Riverin, G., 1995. The subseafloor formation of volcanic-hosted massive sulphides: evidence from the Ansil deposit, Rouyn-Noranda, Canada; Economic Geology and the Bulletin of the Society of Economic Geologists, v. 90, p. 2006–2017. doi:10.2113/gsecongeo.90.7.2006

Galley, A.G., Jonasson, I.R., and Watkinson, D.H., 2000. Magnetite-rich calc-silicate alteration in relation to synvolcanic intrusion at the Ansil volcanogenic massive sulphide deposit, Rouyn-Noranda, Quebec, Canada; Mineralium Deposita, v. 35, p. 619–637. doi:10.1007/s001260050267

Gélinas, L., Trudel, P., and Hubert, C., 1984. Chemostratigraphic division of the Blake River Group, Rouyn-Noranda area, Abitibi, Quebec; Canadian Journal of Earth Sciences, v. 21, p. 220–231.

Gibson, H. and Galley, A., 2007. Volcanogenic massive sulphide deposits of the Archean, Noranda District, Quebec; *in* Mineral deposits of Canada: a synthesis of major deposit types, district metallogeny, the evolution of geological provinces and exploration methods, (ed.) W.D. Goodfellow; Geological Association of Canada, Mineral Deposits Division, Special Publication No. 5, p. 533–552.

Gibson, H.L. and Watkinson, D.H., 1990. Volcanogenic massive sulphide deposits of the Noranda cauldron and shield volcano, Quebec; *in* The northwestern Quebec polymetallic belt, (ed.) M. Rive, P. Verpaelst, Y. Gagnon, J.M. Lulin, G. Riverin, and A. Simard; Canadian Institute of Mining Metallurgy, Special Volume 43, p. 119–132.

Goldie, R., 1978. Magma mixing in the Flavrian pluton, Noranda area, Quebec; Canadian Journal of Earth Sciences, v. 15, p. 132–144.

Goutier, J., McNicoll, V., Dion, C., Lafrance, B., Legault, M., Ross, P.-S., Mercier-Langevin, P., Cheng, L.-Z., de Kemp, E., and Ayer, J., 2009. L'impact du Plan Cuivre et de L'ICG-3 sur la géologie de l'Abitibi et du Groupe de Blake River; *in* Proceedings Volume, Congrès Abitibi 2009 – Abitibi Cuivre, Rouyn-Noranda, September 28th, 2009, p. 9–13.

Larson, J.E., 1983. Geology, geochemistry and wall-rock alteration at the Magusi and New Insco massive sulfide deposits, Hebecourt Township, northwestern Quebec; M.Sc. thesis, University of Western Ontario, London, Ontario, 173 p.

McNicoll, V., Goutier, J., Dion, C., Ross, P.-S., and Mercier-Langevin, P., 2009. Portrait des grandes unites du Groupe de Blake River et leur relation avec les sulfures massifs volcanogènes; *in* Excursion Guidebook, Congrès Abitibi 2009 – Abitibi Cuivre, Rouyn-Noranda, September 28th, 2009, p. 9–28.

Monecke, T., Gibson, H., Dubé, B., Laurin, J., Hannington, M.D., and Martin, L., 2008. Geology and volcanic setting of the Horne deposit, Quebec: initial results of a new research project; Geological Survey of Canada, Current Research 2008-9, 16 p.

Mortensen, J.K., 1987. Preliminary U-Pb zircon ages for volcanic and plutonic rocks of the Noranda-Lac Abitibi area, Abitibi Subprovince, Quebec; *in* Current Research, Part A; Geological Survey of Canada, Paper 87–1A, p. 581–590.

Murowchick, J.B., 1992. Marcasite inversion and the petrographic determination of pyrite ancestry; Economic Geology and the Bulletin of the Society of Economic Geologists, v. 87, p. 1141–1152. doi:10.2113/gsecongeo.87.4.1141

Riverin, G. and Hodgson, C.J., 1980. Wallrock alteration at the Millenbach Cu-Zn mine, Noranda, Quebec; Economic Geology and the Bulletin of the Society of Economic Geologists, v. 75, p. 424–444. doi:10.2113/gsecongeo.75.3.424

Riverin, G., LaBrie, M., Salmon, B., Cazavant, A., Asselin, R., and Gagnon, M., 1990. The geology of the Ansil deposit, Rouyn-Noranda, Quebec; *in* The northwestern Quebec polymetallic belt, (ed.) M. Rive, P. Verpaelst, Y. Gagnon, J.M. Lulin, G. Riverin, and A. Simard; Canadian Institute of Mining Metallurgy, Special Volume 43, p. 143–151.

Westendorp, R.W., 1992. Magnetite zones at the Ansil Cu-Zn deposit, Rouyn-Noranda, Quebec: M.Sc. thesis, Carleton University, Ottawa, Ontario, 46 p.

Westendorp, R.W., Watkinson, D.H., and Jonasson, I.R., 1991. Silicon-bearing zoned magnetite crystals and the evolution of hydrothermal fluid at the Ansil Cu-Zn Mine, Rouyn-Noranda, Quebec; Economic Geology and the Bulletin of the Society of Economic Geologists, v. 86, p. 1110–1114. doi:10.2113/gsecongeo.86.5.1110

Xstrata Copper Canada Ltd., 2005. West Ansil resource estimate; 43-101F1 Technical Report, 50 p.

Geological Survey of Canada Project X91